Ab initio Studies of $NH_4^+(H_2O)_{1-5}$ and the Influence of Hydrogen-Bonding Nonadditivity on Geometries and Vibrations

J. C. Jiang,[†] H.-C. Chang,*[,†] Y. T. Lee,[†,‡] and S. H. Lin[†,‡]

Institute of Atomic and Molecular Sciences, Academia Sinica, P.O. Box 23-166, Taipei, Taiwan 106, Republic of China, and Department of Chemistry, National Taiwan University, Taipei, Taiwan 106, Republic of China

Received: September 24, 1998

Ab initio calculations were performed to investigate the structures, energetics, and vibrations of $NH_4^+(H_2O)_n$ cluster ions at $n = 0-5$. Equilibrium geometries of NH_4^+ and $NH_4^+-H_2O$ are optimized at the MP2, MP4, CCD, QCISD, and B3LYP levels using the 6-31G*, 6-31G**, 6-31+G*, 6-31++G**, 6-311+G**, and 6-311++G** basis sets. The benchmark calculations indicate that using MP2 and B3LYP approaches with the 6-31+G* basis set is well suited for characterizing large $NH_4^+(H_2O)_n$ clusters. The two approaches correspondingly find the existence of a number of structural isomers at $n = 2-5$, of which the isomer with a filled first solvation shell is lowest in energy at $n = 4$. The calculations further predict that, at $n = 5$, the lowest energy isomer contains a four-membered ring with the second-shell H_2O acting as a double-proton acceptor (AA). The prediction is in good agreement with the observation of jet-cooled $NH_4^+(H_2O)_5$, where a characteristic hydrogen-bonded-OH stretching absorption at ~3550 cm^{-1} is identified for the $AA-H_2O$ molecule in the vibrational predissociation spectra (Wang, Y.-S.; Chang, H.-C.; Jiang, J. C.; Lin, S. H.; Lee, Y. T.; Chang, H.-C. *J. Am. Chem. Soc.* **1998**, *102*, 8777). In this study, in addition to energetics, how hydrogen-bonding nonadditivity influences the geometries and vibrations of these clusters is analyzed.

Introduction

Ion−solvent interactions play an important role in a wide range of chemical and biological systems. The importance is particularly evident in aqueous solutions where the interactions involve hydrogen bonding.[1] To better understand the nature of ion hydration, extensive experimental[2−6] and theoretical[7−19] investigations of cluster ions in the gas phase have been performed over the past few decades. The commonly used experimental techniques are mass spectrometry[2,3] and laser spectroscopy.[4−6] The former provides useful information about the strength of binding between solvent molecules and ion cores whereas the latter reveals structural details. Presently, a large body of thermochemical data about ion hydration exists in the literature;[2,3] however, the number of spectroscopic measurements is limited owing to experimental difficulties.[20] Theoretical calculations offer an alternative approach in increasing our understanding of ion−solvent interactions. Recent advances in ab initio calculations have allowed the structures, binding energies, and vibrational frequencies of molecular clusters to be fairly accurately predicted.[7−19] The calculations not only serve as a useful reference for comparison with experiments but also furnish a complete picture of the structures and dynamics of the clusters of interest.

The density functional theory (DFT) has recently been recognized as a useful method for studying extended systems, such as clusters. The method possesses an attractive feature of being less computationally demanding when including electron correlation in the computation. To date, most of the DFT applications focus on the study of structures, proton affinities, electron affinities, binding energies, isomeric transitions, vibrational frequencies, internal rotations, and chemical reactions of neutral molecular systems;[21] only a few applications attempt to elucidate ion−solvent interactions. In this study, we chose to investigate ammonium ion−water clusters, which are abundant in the biosphere.[22] The ammonium ion (NH_4^+), heavily involved in various biological and chemical reactions, is one the most important ionic species in aqueous solutions. In spite of its importance, our current knowledge of how the ammonium ion interacts with water molecules remains incomplete, and most of the existing work concerns only the interactions within the binary complex $NH_4^+-H_2O$.[11] The lack of knowledge of extended systems motivated us to study $NH_4^+(H_2O)_{2-5}$ using DFT-based ab initio calculations. It is found in these clusters that the interaction energies, structures, and vibrational frequencies are strongly influenced by the coupling between hydrogen bonds. The hydrogen bonding nonadditivity, also known as the hydrogen-bond (HB) cooperative effect in many macromolecules, condensed phases, and aqueous solutions,[23−28] is analyzed in detail in the present calculations.

Previous thermochemical measurements[2,3] revealed a smooth decrease in the heat of hydration ($\Delta H_{n-1,n}$) for the clustering, $NH_4^+(H_2O)_{n-1} + H_2O \rightarrow NH_4^+(H_2O)_n$, as n increases from 2 to 6. The absence of an abrupt change between $\Delta H_{3,4}$ and $\Delta H_{4,5}$ suggests that structural isomerization can occur at $n = 4$ when the first hydration is to be filled. This is indeed verified by Wang et al.,[6] who found a number of structural isomers for $NH_4^+(H_2O)_{4-6}$ in a supersonic jet using vibrational predissociation spectroscopy. Interestingly, at $n = 5$, the spectra in the hydrogen-bonded−OH stretching region indicate that the most stable isomeric form of $NH_4^+(H_2O)_5$ comprises a symmetric four-membered ring with the fifth water molecule acting as a double-proton acceptor on the second solvation shell. This structure was not previously predicted by Armstrong et al.,[7] who

[†] Institute of Atomic and Molecular Sciences, Academia Sinica.
[‡] National Taiwan University.

10.1021/jp9838543 CCC: $18.00
Published on Web 04/07/1999

calculated the structures and energetics of $NH_4^+(H_2O)_n$ up to $n = 5$. In the HF/6-31+G* calculations, they considered mainly charge−dipole interactions, which are insufficient to account for the complex couplings involved in these clusters.

In this study, we carried out both DFT and conventional ab initio calculations to interpret the spectroscopic observations of $NH_4^+(H_2O)_n$.[6] We calculated the total interaction energy of the reaction $NH_4^+ + nH_2O \rightarrow NH_4^+(H_2O)_n$ and the stepwise hydration energy of $NH_4^+(H_2O)_{n-1} + H_2O \rightarrow NH_4^+(H_2O)_n$. Also explored in the calculations was the dependence of the structures, hydration energies, and vibrational frequency shifts on the number of solvent molecules; how these properties are influenced by the attachment of outer shell solvent molecules was investigated. The predicted spectra, containing information of both vibrational frequencies and absorption intensities, of the OH stretching of the solvent molecules and the NH stretching of the ion core are presented for $NH_4^+(H_2O)_{1-5}$.

Methods

The ab initio calculations were performed using the commercial Gaussian 94 package.[29] Equilibrium geometries of the NH_4^+ and $NH_4^+-H_2O$ ions were optimized at the MP2, CCD, QCISD, and B3LYP levels using the 6-31G*, 6-31G**, 6-31+G*, 6-31++G**, 6-311+G**, and 6-311++G** basis sets as the benchmark calculations. For larger clusters, such as $NH_4^+(H_2O)_{2-5}$, the geometric parameters were obtained at the MP2 and B3LYP levels using 6-31+G*. Most of the optimizations were symmetry-unconstrained with the binding energies corrected by zero-point vibrational energy (ZPVE) and basis set superposition errors (BSSE) following the procedures of Boys−Bernardi.[30] The BSSE corrections for the stepwise and the total hydration energies were made as follows:

(1) The stepwise hydration, $AW_{n-1} + W \rightarrow AW_n$,

$$E(\text{BSSE}) = [E(AW_{n-1})_n - E(AW_{n-1})] + [E(W_n)_n - E(W)]$$

(2) The total hydration, $A + nW \rightarrow AW_n$,

$$E(\text{BSSE}) = [E(A)_n - E(A)] + \sum_{i=1}^{n} [E(W_i)_n - E(W_i)]$$

where $E(AW_{n-1})_n$, $E(W_i)_n$, and $E(A)_n$ represent the energies of $NH_4^+(H_2O)_{n-1}$, $(H_2O)_i$, and NH_4^+ calculated using their geometries within the clusters, and $E(AW_{n-1})_{n-1}$, $E(W_i)$, and $E(A)$ are the energies of the individual clusters and ions with the basis functions centered on themselves. A complete set of basis functions was employed to describe AW_n.

In this presentation, the factors used to scale the calculated frequencies are 0.973 and 0.969 for B3LYP/6-31+G* and MP2/6-31+G*, respectively. They were chosen by referring to the experimentally observed free-OH stretching frequencies of two- and three-coordinated H_2O molecules in these clusters.[6a]

Results and Discussion

To simplify the following discussions, we characterize the water molecules, either in the first (1°) or the second (2°) solvation shell of the NH_4^+ ion core, according to their hydrogen bonding: single-acceptor (A), single-donor (D), double acceptor (AA), double-donor (DD), single-acceptor-single-donor (AD), single-acceptor-double-donor (ADD), double-acceptor-single-donor (AAD), and double-acceptor-double-donor (AADD).[31] The water molecules are also labeled using parentheses (W1, W2, ···, or W*n*) on the basis of their positions. Depending on how hydrogen bonding is made, the NH and OH groups are prefixed with b or f representing, respectively, hydrogen-bonded or non-hydrogen-bonded (free) states. In comparing the calculated results, both the B3LYP/6-31+G* and MP2/6-31+G* values are listed but with the latter given in parentheses.

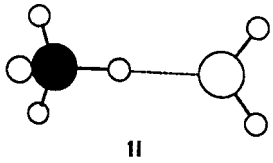

1I

Figure 1. Ab initio optimized structures of $NH_4^+(H_2O)$. The N, O, and H atoms are denoted by ●, ○, and ◦, respectively.

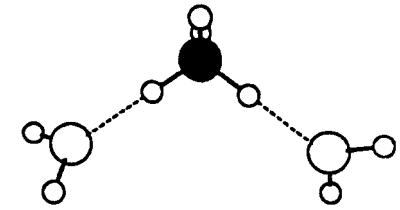

2I

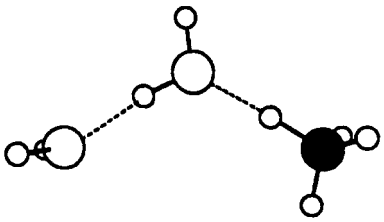

2II

Figure 2. Ab initio optimized structures of $NH_4^+(H_2O)_2$. The N, O, and H atoms are denoted by ●, ○, and ◦, respectively.

A. Geometries and Energetics. A number of local minima exist in the potential energy surfaces of $NH_4^+(H_2O)_{1-5}$. Figures 1−5 illustrate some representative structures of these potential minima. Table 1 lists the corresponding energies with and without the BSSE and ZPVE corrections at both the MP2/6-31+G* and B3LYP/6-31+G* levels, from which the total and stepwise interaction energies given in Tables 2 and 3 were obtained. Tables 4−6 list the respective geometric parameters of $NH_4^+(H_2O)_{1-3}$. The salient features of these clusters, presumably formed by successive addition of water molecules to the ammonium ion core, are discussed below.

A.1. $NH_4^+(H_2O)$. Three geometric configurations are found on the interaction hypersurfaces of $NH_4^+(H_2O)$.[9e] They are (1) direct, (2) bisecting, and (3) axial structures, where the oxygen atom of H_2O approaches the ion core either along the direction of the NH bond, along the bisector of the angle held by the two NH bonds, or along the C_{3v} symmetry axis of the plane defined by the three hydrogen atoms, respectively. These structures have been scrupulously investigated in previous ab initio calculations.[8,9d,9e] It has been found that the complexion via direct hydrogen bonding yields a structure of the lowest in energy. The structure (with C_1 symmetry) is predominantly determined by charge−dipole interactions. Table 4 lists the geometric parameters of NH_4^+ and this binary complex, where the N−H···O hydrogen bond is shown to lie in the plane defined by the H_2O with a bond angle of $\angle$N−H···O ∼ 180°. Compared to that of NH_4^+, the proton-donating N−H bond (denoted as b-NH) is lengthened by ∼0.03 Å and the free N−H bonds (denoted as f-NH) are shortened by ∼0.003 Å. The predicted

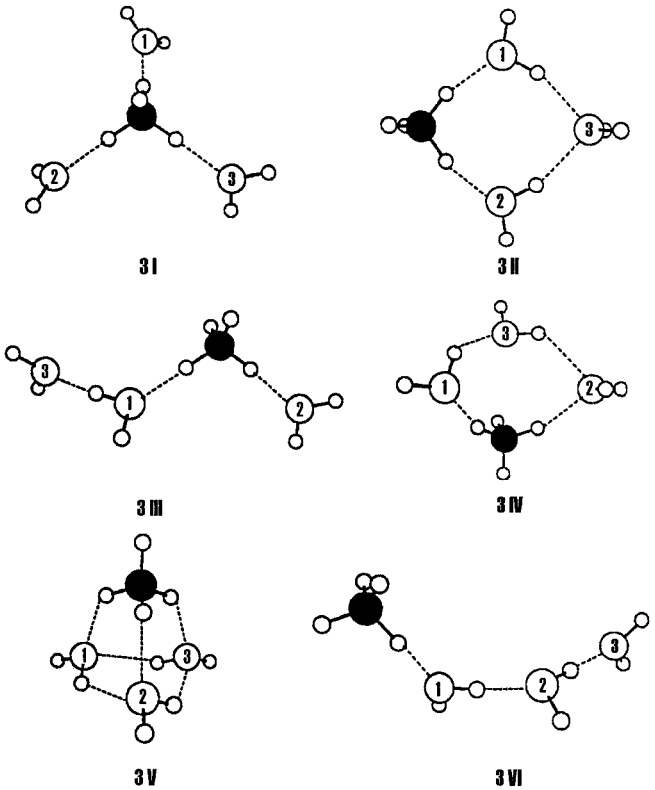

Figure 3. Ab initio optimized structures of $NH_4^+(H_2O)_3$. The N, O, and H atoms are denoted by ●, ○, and ◦, respectively.

N···O distance is 2.728 (2.766) Å, which is considerably shorter than the typical separation of ~4 Å in neutral van der Waals complexes.

Table 2 compares the binding energies with and without the BSSE and ZPVE corrections of structure **1I** at various computational levels. They are performed in an effort to find a reliable and economical method for predicting the properties of larger clusters. The calculated final interaction energy at the higher levels is found to converge at $-\Delta E_f \sim 17.5$ kcal/mol, a value which is slightly overestimated by MP2 using the 6-31+G*, 6-31++G**, 6-311+G**, and 6-311++G** basis sets. It appears that the use of basis sets that are more flexible than 6-31+G* does not substantially improve the accuracy of the MP2 calculations. However, if diffuse functions are not imposed on the heavier atoms, considerable overestimation of the hydration energy can be made by MP2. As for DFT, when using the same basis sets, the B3LYP functional overestimates the interaction energy for more than 1 kcal/mol. Similar to that of MP2, the use of more flexible basis sets only slightly improves the results of this calculation. Comparing the calculated with the measured values shown in Table 2 reveals that the MP2/6-31+G* method can already provide sufficiently accurate estimates for the interaction energy of NH_4^+ and H_2O. Unfortunately, application of this method to larger clusters is still impractical at present since extensive disk space is required. The DFT is the alternative. To test the validity of the B3LYP method in elucidating ion−molecule interactions, calculations at both the B3LYP/6-31+G* and MP2/6-31+G* levels were performed and compared for clusters with a size of $n = 2-5$.

A.2. $NH_4^+(H_2O)_2$. The most energetically favored approach for the second H_2O to $NH_4^+(H_2O)$ is via the formation of an additional N−H···O hydrogen bond. As illustrated in Figure 2, the optimized geometry of this isomer (**2I**) has a C_1 (C_s) symmetry, predicted by B3LYP/6-31+G* (MP2/6-31+G*),

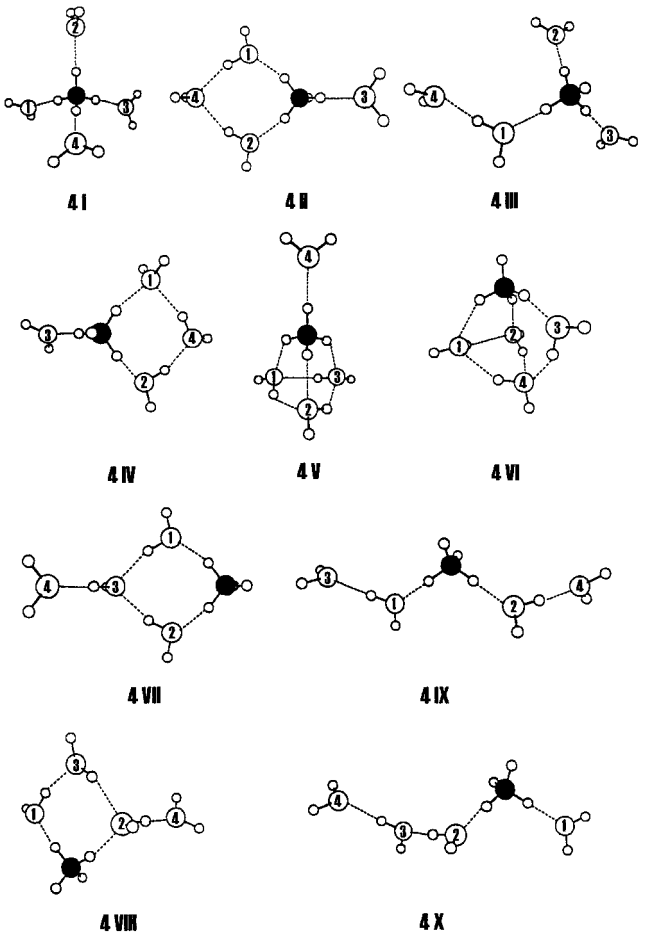

Figure 4. Ab initio optimized structures of $NH_4^+(H_2O)_4$. The N, O, and H atoms are denoted by ●, ○, and ◦, respectively.

where the b-NH and the two f-OH bonds involved in each hydrogen bonding lie in the same plane with an angle of ∠O···H−N ~ 180°. In $NH_4^+(H_2O)_2$, the second hydrogen bond can also be formed between the two H_2O molecules, giving rise to isomer **2II** which has an energy about 3 kcal/mol higher than that of **2I** (cf. Table 3). Table 5 lists the geometric parameters of these two isomers. In **2I**, the bond length of each b-NH is slightly decreased by ~0.01 Å, and the N···O distances are increased by ~0.05 Å, compared to those of **1I**. For isomer **2II**, however, the same comparison reveals that it has a bond length increase of more than 0.01 Å in b-NH, and a N···O distance decrease of ~0.08 Å. Also noteworthy in **2II** is that the O···O separation of 2.705 (2.746) Å is significantly shorter than the calculated 2.877 (2.906) Å of the neutral water dimer,[32] and the predicted N−H···O hydrogen bonding energy of 29.19 (27.15) kcal/mol is considerably larger than that of **1I**. Furthermore, the predicted O−H···O bond strength of 12.66 (11.46) kcal/mol is nearly five-fold larger than 2.79 (2.42) kcal/mol of $(H_2O)_2$.[32] The dramatic increase of the N−H···O and O−H···O bonding energies in **2II** indicates that the extent of electron transfer in these two hydrogen bonds is greatly augmented upon complexion.

Comparison of the calculated results between isomers **2I** and **2II** reveals the importance of HB cooperativity in determining the molecular properties of protonated ion−water clusters. In isomer **2I**, the total interaction energy contained by the two N−H···O hydrogen bonds is 34.73 (32.94) kcal/mol, which is less than twice the N−H···O bonding energy of **1I** by 3.63 (2.96) kcal/mol. In contrast, the total interaction energy contained by **2II** in the N−H···O and O−H···O bonds is 31.73

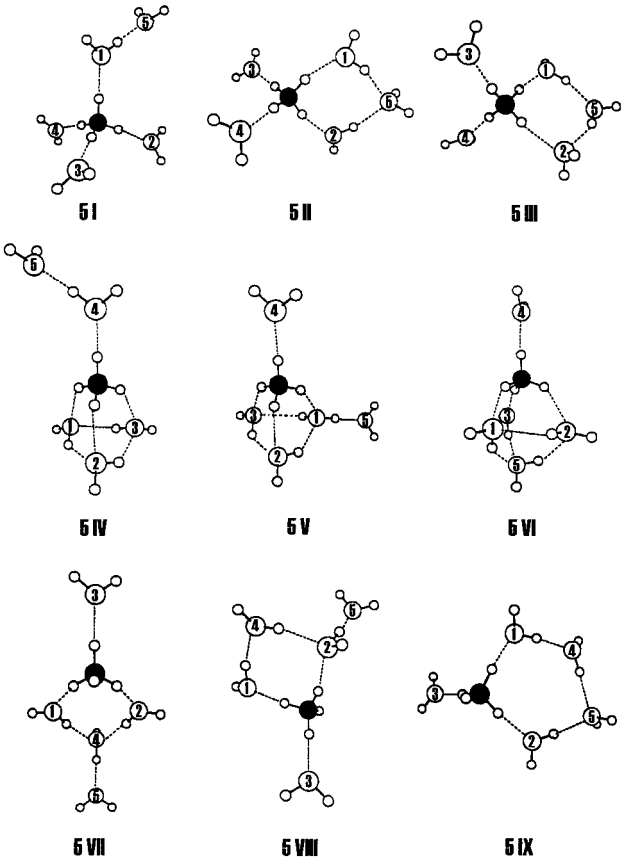

Figure 5. Ab initio optimized structures of $NH_4^+(H_2O)_5$. The N, O, and H atoms are denoted by ●, ○, and ◦, respectively.

(29.14) kcal/mol, which is larger than the sum of the interaction energies of N−H···O in isomer **1I** and O−H···O in $(H_2O)_2$ by 9.76 (8.77) kcal/mol. The increase in interaction energy, together with the elongation of the b-NH bond and the reduction of the N···O and O···O distances, indicates that the N−H···O and the O−H···O hydrogen bonds are cooperatively coupled in isomer **2II**. This is opposite to the anticooperative case of **2I**, where the b-NH bonds shorten, the N···O distances increase and the interaction energy is negatively nonadditive when the second H_2O molecule attaches to the ion core. It is now well-known that the HB cooperativity due to concerted charge transfer can greatly enhance the strength of the individual hydrogen bonds involved in the coupling.[33,34] In isomer **2I**, where the NH_4^+ ion acts as a double proton donor bridging two water molecules, the extent of charge transfer between NH_4^+ and either H_2O is reduced, resulting in weaker N−H···O hydrogen bonding compared to that of **1I**. As in isomer **2II**, where the 1°H_2O functions both as a proton donor and as a proton acceptor in a linear linkage, the strength of each N−H···O and O−H···O hydrogen bond is augmented due to the concerted coupling. Although strongly favored by the HB cooperativity, isomer **2II** remains less stable than **2I** since the O−H···O hydrogen bonding is much weaker than that of N^+−H···O.

A.3. $NH_4^+(H_2O)_3$. The $NH_4^+(H_2O)_3$ cluster ion contains a number of energy minima in the interaction potential. Figure 3 depicts the low-energy structures of the isomers with geometric parameters listed in Table 6. Among these isomers, one of the lowest in energy is **3I**, in which NH_4^+ forms three hydrogen bonds with three geometrically equivalent H_2O molecules. The NH_4^+ ion in this cluster behaves like a triple proton donor. The behavior diminishes the extent of charge transfer from the ion core to each solvent molecule, thereby weakening each N−H···O hydrogen bond. Compared to **2I** and **1I**, this isomer has a shorter b-NH bond length, accompanied by an increased N···O distance. The b-NH and the two f-OH bonds of each hydrogen bonding remain coplanar with an angle of ∠N−H···O ∼ 180°. Notably, the energy of the hydration (**2I** + H_2O → **3I**) is ∼13 kcal/mol, which is smaller than ∼15 kcal/mole of (**1I** + H_2O → **2I**) and ∼19 kcal/mole of (NH_4^+ + H_2O → **1I**).

Two additional isomers (**3II** and **3III**) are considered for $NH_4^+(H_2O)_3$. The symmetric, ring-shaped isomer (**3II**) is ∼2 kcal/mol less stable than **3I** and is the second lowest in energy. In this isomer, the water molecule situated on the second solvation shell (2°) acts as a double-proton acceptor (AA), forming two equivalent O−H···O hydrogen bonds with the two single-acceptor-single-donor (AD) H_2O molecules on the first solvation shell (1°). The two b-NH and the four OH bonds all lie in the same plane composed by the four hydrogen bonds involving the two AD−1°H_2O molecules. The angle contained by the two N−H bonds is tightened by 4° because of the four-membered ring formation. Owing to the HB cooperativity between N−H···O and O−H···O, the b-NH bond length of 1.052 (1.045) Å is slightly longer than that of **2I**, and the N···O distance of 2.732 (2.757) Å is slightly shorter than that of **2I**. As for O···O, the average separation of 2.862 (2.895) Å is significantly larger than the corresponding one in **2II**, a result of anticooperative couplings between the two O−H···O hydrogen bonds. Although isomer **3II** has one more hydrogen bond than **3I**, it is one bond less in N−H···O and thus is relatively not favored in energy.

Two data sets concerning the bond length of b-NH and the distance of N···O exist for **3III**, and they are exactly out of phase as compared to those of **2I**. In one set where the O−H···O hydrogen bond is cooperative with N−H···O, the b-NH bond is lengthened, and the N···O distance is shortened. This involves bonding of the water dimer (Wl + W3) to the ion core. In another set where the HB anticooperativity persists due to water monomer (W2) attachment, the changes in geometry are similar to that of **1I** → **2I**: the b-NH bond is shortened and the N···O distance is lengthened. The equilibrium geometry of this cluster **3III** is, thus, a result of the delicate balance between these two competitive effects. Note that, while the number of O−H···O hydrogen bonds in **3III** is lower than that in **3II** by one, they are comparable in terms of stability. This is primarily due to the loss of hydrogen bond directionality, which reduces the bond strength,[31] upon ring formation in **3II**.

In the course of performing calculations, MP2/6-31+G* collapsed on isomer **3IV**, which consists of an asymmetric four-fold ring. This isomer, however, is predicted to be stable by B3LYP/6-31+G*. Differing from **3II**, it contains an AA−1°H_2O, instead of an AA−2°H_2O. The potential well of this isomer is relatively shallow, with a minimum which is ∼5 kcal/mol higher than that of **3I**. Also due to the difference in hydrogen bonding nonadditivity, two distinct data sets on bond lengths and internuclear distances exist: 1.059, 2.670, and 2.754 Å versus 1.040, 2.892, and 2.915 Å for b-NH, N···O, and O···O, respectively. In this isomer, the l°H_2O (W2) no longer lies in the same plane with b-NH, indicating that the interaction between the b-NH dipole and the electron lone pair of O is the dominant intermolecular force in this case. Interestingly, while the number of hydrogen bonds is the same and the degree of losing hydrogen bond directionality is similar between **3II** and **3IV**, the latter is 3.5 kcal/mol less stable because the dipole−electron lone pair interaction is much weaker than the charge−dipole interaction.

TABLE 1: Energies (hartree) of $NH_4^+(H_2O)_n$ at $n = 0-5$.

	B3LYP/6-31+G*			MP2/6-31+G*		
structures	E	E_{zpve}[a]	E_f[b]	E	E_{zpve}[a]	E_f[b]
H_2O	−76.422 572 3	−76.401 476		−76.209 776 6	−76.188 532	
NH_4^+	−56.894 586 0	−56.844 686		−56.701 165 8	−56.650 671	
1I	−133.352 458 5	−133.278 527	−133.276 722	−132.946 353 6	−132.871 481	−132.867 802
2I	−209.804 435 4	−209.706 472	−209.702 984	−209.186 574 3	−209.087 339	−209.080 231
2II	−209.800 504 0	−209.702 219	−209.698 188	−209.181 898 6	−209.082 203	−209.074 181
3I	−286.252 050 9	−286.130 387	−286.125 246	−285.422 959 5	−285.299 643	−285.289 203
3II	−286.253 116 9	−286.128 585	−286.122 197	−285.424 225 9	−285.298 283	−285.285 572
3III	−286.250 003 8	−286.127 600	−286.121 991	−285.420 033 7	−285.296 031	−285.284 798
3IV	−286.247 112 2	−286.122 482	−286.116 586			
3V	−286.246 591 7	−286.121 390	−286.115 792	−285.420 415 0	−285.293 729	−285.282 082
3VI	−286.243 593 7	−286.121 060	−286.114 821	−285.412 694 6	−285.288 559	−285.276 405
4I	−362.695 994 2	−362.550 927	−362.544 061	−361.656 046 4	−361.509 075	−361.495 229
4II	−362.698 969 4	−362.550 921	−362.542 889	−361.659 012 6	−361.509 250	−361.493 268
4III	−362.695 425 0	−362.549 232	−362.542 027	−361.654 423 9	−361.506 464	−361.492 069
4IV	−362.693 964 0	−362.545 536	−362.537 453			
4V	−362.694 190 7	−362.544 672	−362.537 344	−361.656 535 8	−361.505 651	−361.490 465
4VI	−362.696 274 0	−362.545 473	−362.537 078	−361.657 783 6	−361.505 729	−361.488 835
4VII	−362.698 317 9	−362.549 749	−362.540 965	−361.657 447 6	−361.506 999	−361.489 666
4VIII	−362.693 752 4	−362.544 424	−362.535 642			
4IX	−362.694 402 2	−362.547 613	−362.539 906	−361.652 491 5	−361.503 810	−361.488 558
4X	−362.691 920 3	−362.545 146	−362.537 392	−361.649 873 5	−361.501 323	−361.486 038
5I	−439.137 873 6	−438.968 206	−438.959 377	−437.886 160 4	−437.714 516	−437.696 787
5II	−439.141 645 0	−438.970 072	−438.960 490	−437.890 872 4	−437.717 469	−437.698 155
5III	−439.137 830 8	−438.965 797	−438.955 978	−437.886 413 5	−437.712 830	−437.693 601
5IV	−439.137 663 0	−438.963 593	−438.954 162	−437.888 017 0	−437.712 267	−437.693 021
5V				−437.887 725 1	−437.712 639	−437.693 215
5VI	−439.141 692 5	−438.967 112	−438.957 066	−437.892 072 4	−437.716 076	−437.695 632
5VII	−439.143 181 2	−438.971 085	−438.960 788	−437.891 356 4	−437.717 105	−437.696 588
5VIII	−439.139 580 5	−438.966 234	−438.955 872			
5IX	−439.141 002 3	−438.968 150	−438.957 704	−437.889 067 6	−437.714 588	−437.694 145

[a] With ZPVE corrections. [b] With both ZPVE and BSSE corrections.

TABLE 2: First Hydration Energies (kcal/mol) of NH_4^+

methods	$-\Delta E$	$-\Delta E_{cp}$	$-\Delta E_{zpve}$	$-\Delta E_f$
B3LYP/6-31G*	25.31	24.11	23.71	22.51
B3LYP/6-31+G*	22.15	21.02	20.31	19.18
B3LYP/6-31G**	25.64	24.30	24.17	22.77
B3LYP/6-31+G*	22.11	21.15	20.30	19.34
B3LYP/6-31+G**	22.02	21.20	20.15	19.33
B3LYP/6-311++G**	22.01	21.17	20.13	19.29
MP2/6-31G*	24.21	22.63	22.41	20.83
MP2/6-31+G*	22.22	19.91	20.25	17.95
MP2/6-31G**	24.21	22.49	22.54	20.83
MP2/6-31++G**	21.74	19.75	19.88	17.88
MP2/6-311+G**	21.61	19.74	19.80	17.93
MP2/6-311++G**	21.61	19.71	19.81	17.91
MP4/6-311++G**(D)[a,b]	21.15	19.31	19.35	17.51
MP4/6-311++G**(SD)[a,b]	20.96	19.18	19.16	17.38
MP4/6-311++G**(SDQ)[a,b]	21.00	19.17	19.20	17.37
MP4/6-311++G**(SDTQ)[a,b]	21.34	19.34	19.54	17.54
CCD/6-311++G**[b]	20.92	19.31	19.12	17.51
QCISD/6-311++G**[b]	20.95	20.62	19.15	17.82
exptl		19.9,[c] 17.2,[d] 17.3[e]		

[a] Of the MP2/6-311++G** geometries. [b] ZPVE corrections made based upon the MP2/6-311++G** geometries. [c] Reference 3. [d] Reference 2b. [c] Reference 3. [d] Reference 2b. [e] Reference 2a.

Isomer **3V** is formed by attaching a cyclic water trimer to the ammonium ion core via three N−H···O hydrogen bonds. The size of the water trimer is slightly expanded with an average O···O distance of 2.87 (2.87) Å and an average angle of ∠O−H···O ∼ 125.2° (124.5°), compared to the corresponding values of 2.771 Å and 149.1° for isolated cyclic $(H_2O)_3$.[32] In order to form this isomer, the linearity of the three N−H···O hydrogen bonds must be reduced to ∠N−H···O ∼ 134° (133°). Although isomer **3V** possesses three N−H···O and three O−H···O hydrogen bonds, it is higher in energy than **3I** by 5.93 (4.47) kcal/mol because of the loss of hydrogen bond directionality in both N−H···O and O−H···O.

Calculations of the linear isomer **3VI** were conducted to explore the long-range influence of the ion core. Owing to the increased HB cooperativity, the b-NH bond is further lengthened and the N−H···O bond is shortened. Compared to that of **2II**, the interoxygen separation in **3VI** is shorter by 0.071 (0.067) Å for $O_1\cdots O_2$. This means that adding one more H_2O to the end of the water chain strengthens the hydrogen bonding between 1°H_2O and 2°H_2O. The $O_2-H\cdots O_3$ bond, however, is relatively weaker because the 3°H_2O molecule is situated further away from the ion core. The predicted hydration energy of (**2II** + $H_2O \rightarrow$ **3VI**) is 9.69 (8.88) kcal/mol, which is substantially larger than that in neutral water clusters, suggesting that the ion core continues to influence the bonding of the 3°-H_2O molecule. It is interesting to note that the interaction energy of $O_1-H\cdots O_2$ in this linear chainlike isomer is surprisingly large, 19.62 (17.99) kcal/mol, which signifies the important role the HB cooperative effect plays in hydrogen-bonded systems.

A.4. $NH_4^+(H_2O)_4$. Isomer **4I** presents itself as the most stable structure of $NH_4^+(H_2O)_4$; it contains an ion core with a complete solvation shell. Other isomers of comparable stability can also be found in Table 3, where **4I**, **4II**, and **4III** are within 2 kcal/mol of each other in energy. Previous vibrational predissociation spectroscopy of $NH_4^+(H_2O)_4$ reveals three isomers in a supersonic jet, and they were identified as **4I**, **4II**, and **4III** based upon their characteristic vibrational signatures.[6b] Systematic investigations of the temperature-dependent spectra indicate that the isomers are stable in the order of **4I** > **4II** > **4III**. This experimental observation is in good agreement with the calculated energies listed in Table 3. Note that, for these three isomers, the respective stepwise hydration energies of (**3I** + $H_2O \rightarrow$ **4I**), (**3I** + $H_2O \rightarrow$ **4II**) and (**3I** + $H_2O \rightarrow$ **4III**) are all

TABLE 3: Total and Stepwise Hydration Energies[a] kcal/mol) of [$NH_4^+ + nH_2O \rightarrow NH_4^+(H_2O)_n$] and [$NH_4^+(H_2O)_{n-1} + H_2O \rightarrow NH_4^+(H_2O)_n$] Estimated by B3LYP/6-31+G* and MP2/6-31+G*

	B3LYP/6-31+G*		MP2/6-31 +G*	
$NH_4^+(H_2O)_n$	$-\Delta E_n$	$-\Delta E_{n-1,n}$[b]	$-\Delta E_n$	$-\Delta E_{n-1,n}$[b]
1I	19.18		17.95	
2I	34.73	15.52 (**1I**)	32.94	14.88 (**1I**)
2II	31.73	12.66 (**1I**)	29.14	11.46 (**1I**)
3I	47.77	13.02 (**2I**)	45.77	12.65 (**2I**)
3II	45.86	11.05 (**2I**)	43.49	10.45 (**2I**)
3III	45.73	11.10 (**2I**), 13.94 (**2II**)	43.01	10.25 (**2I**), 13.66 (**2II**)
3IV	42.34	7.58 (**2I**)		
3V	41.84		41.30	
3VI	41.23	9.69 (**2II**)	37.74	8.88 (**2II**)
4I	58.65	10.81 (**3I**)	56.74	10.76 (**3I**)
4II	57.92	10.07 (**3I**), 11.98 (**3II**)	55.51	9.62 (**3I**), 11.81 (**3II**)
4III	57.38	9.69 (**3I**), 11.56 (**3III**)	54.76	9.12 (**3I**), 11.51 (**3III**)
4IV	54.51	12.44 (**3IV**)		
4V	54.44	12.63 (**3V**)	53.75	12.38 (**3V**)
4VI	54.27		52.73	
4VII	56.71	11.12 (**3II**)	53.25	10.21 (**3II**)
4VIII	53.37	11.57 (**3IV**)		
4IX	56.04	10.46 (**3III**)	52.55	9.70 (**3III**)
4X	54.46	8.73 (**3III**)	50.97	8.24 (**3III**)
5I	67.34	8.76 (**4I**), 9.89 (**4III**)	64.92	8.29 (**4I**), 9.91 (**4III**)
5II	68.04	9.22 (**4I**), 10.04 (**4II**)	65.78	9.03 (**4I**), 10.00 (**4II**)
5III	65.20	6.53 (**4I**), 10.66 (**4IV**)	62.92	6.09 (**4I**)
5IV	64.06	9.73 (**4V**)	62.56	8.99 (**4V**)
5V			62.68	9.11 (**4V**)
5VI	65.86	11.59 (**4VI**)	64.20	11.37 (**4VI**)
5VII	68.18	10.51 (**4II**), 11.37 (**4VII**)	64.80	9.70 (**4II**), 11.28 (**4VII**)
5VIII	65.18	10.87 (**4VI**), 7.85 (**4III**), 11.27 (**4X**)		
5IX	66.26	8.99 (**4III**)	63.26	8.59 (**4III**)

[a] With BSSE and ZPVE corrections. [b] Notations in parentheses denoting the isomers of $NH_4^+(H_2O)_{n-1}$.

TABLE 4: Geometric Parameters of NH_4^+ and $NH_4^+(H_2O)$[a]

structures	B3LYP/6-31+G*	MP2/6-31+G*
NH_4^+	d(NH) = 1.0293, ∠HNH = 109.47	d(NH) = 1.0287, ∠HNH = 109.47
1I	d(NH) = 1.0625, 1.0264; D(NO) = 2.7284; ∠HNH = 109.99, 109.87, 109.97; 109.09, 109.06, 108.83; ∠NHO = 179.64	d(NH) = 1.0529, 1.0261; D(NO) = 2.7660; ∠HNH = 109.95, 109.86, 109.92; 109.07, 109.15, 108.87; ∠NHO = 179.75

[a] The bond lengths are in unit of angstroms and angles in degrees.

TABLE 5: Geometric Parameters of $NH_4^+(H_2O)_2$[a]

structures	B3LYP/6-31+G*	MP2/6-31+G*
2I	d(NH) = 1.050, 1.025; D(NO) = 2.785, 2.784; ∠HNH = 110.57; ∠NHO = 179.01, 179.02	d(NH) = 1.043, 1.025; D(NO) = 2.814; ∠HNH = 110.28; ∠NHO = 179.62
2II	d(NH) = 1.082, 1.025; D(NO) = 2.646; D(OO) = 2.705; ∠NHO = 178.21; ∠OHO = 173.47	d(NH) = 1.066, 1.024; D(NO) = 2.686; D(OO) = 2.746; ∠NHO = 177.91; ∠OHO =173.79

[a] The bond lengths are in unit of angstroms and angles in degrees.

slightly smaller than those of (**2I** + $H_2O \rightarrow$ **3I**), (**2I** + $H_2O \rightarrow$ **3II**), and (**2I** + $H_2O \rightarrow$ **3III**). This property reflects that both the charge delocalization of the ion core and the HB anticooperativity are reinforced by the additional N−H···O formation. Other than this, the general features of these three isomers closely resemble those of **3I**, **3II**, and **3III**.

Isomers **4IV**, **4V**, and **4VI** are similar in energies but are ∼4 kcal/mol less stable than **4I**, according to B3LYP/6-31+G*. The calculation for the ring-shaped isomer **4IV** collapsed when MP2/6-31+G* was used. Similar to **3V**, isomer **4V** contains a cyclic water trimer but with a complete solvation shell. Owing to the distortion of the hydrogen bonds in the ring, it is considerably higher in energy than **4I**. For isomer **4VI**, the intermolecular interaction is complicated by the presence of roughly three independent units: a water monomer, a water trimer, and an ammonium ion core. A single O−H···O hydrogen bond bridges the water monomer and the trimer, which are linked to the ammonium ion by one and two N−H···O hydrogen bonds, respectively.

Two channels are available for the fourth H_2O to approach isomer **3II**. This approach can proceed through either linking to the f-NH of NH_4^+ or the 2°H_2O of **3II**. The former leads to the formation of isomer **4II** and the latter to that of **4VII**. Energetics calculations of these two species reveal that the 3°H_2O in **4VII** maintains a fairly strong bonding with the 2°H_2O molecule; hence, the hydration energy [11.12 (10.21) kcal/mol] of (**3II** + $H_2O \rightarrow$ **4VII**) is comparable to that [11.98 (11.81) kcal/mol] of (**3II** + $H_2O \rightarrow$ **4II**).

Upon attaching one more H_2O to **3III**, three isomers (**4III**, **4IX**, and **4X**) can be produced, and their geometries depend on how hydrogen bonds are formed. The species **4III**, which is considerably lower in energy than the other two, has been previously observed by means of vibrational predissociation spectroscopy in a supersonic jet.[6b] The symmetric chainlike

TABLE 6: Geometric Parameters of $NH_4^+(H_2O)_3$[a]

structures	B3LYP/6-31+G*	MP2/6-31+G*
3I	$d(NH_{1,2,3}) = 1.043$, $d(NH) = 1.023$; $D(NO) = 2.832$; $\angle NHO = 179.25, 179.23, 179.23$	$d(NH_{1,2,3}) = 1.038$, $d(NH) = 1.023$; $D(NO) = 2.855$; $\angle NHO = 179.27, 179.26, 179.32$
3II	$d(NH_{1,2}) = 1.052$, $d(NH) = 1.023$; $D(NO_{1,2}) = 2.732$; $D(O_1O_3) = 2.861$, $D(O_2O_3) = 2.862$; $\angle NHO_1 = 162.08$, $\angle NHO_2 = 162.06$; $\angle O_1HO_3 = 159.83$, $\angle O_2HO_3 = 159.85$; $\angle H_1NH_2 = 105.90$	$d(NH_{1,2}) = 1.045$, $d(NH) = 1.023$; $D(NO_{1,2}) = 2.757$; $D(O_1O_3) = 2.890$, $D(O_2O_3) = 2.899$; $\angle NHO_1 = 161.04$, $\angle NHO_2 = 161.05$; $\angle O_1HO_3 = 161.07$, $\angle O_2HO_3 = 161.06$; $\angle H_1NH_2 = 105.97$
3III	$d(NH_1) = 1.063$, $d(NH_2) = 1.046$, $d(NH) = 1.024$; $D(NO_1) = 2.707$, $D(NO_2) = 2.805$; $D(O_1O_2) = 2.733$; $\angle NH_1O_1 = 178.01$, $\angle NH_2O_2 = 178.70$; $\angle O_1HO_3 = 174.26$; $\angle H_1NH_2 = 110.72$	$d(NH_1) = 1.053$, $d(NH_2) = 1.041$, $d(NH) = 1.024$; $D(NO_1) = 2.739$, $D(NO_2) = 2.830$; $D(O_1O_2) = 2.769$; $\angle NH_1O_1 = 177.66$, $\angle NH_2O_2 = 179.06$; $\angle O_1HO_3 = 174.46$.; $\angle H_1NH_2 = 110.68$
3IV	$d(NH_1) = 1.059$, $d(NH_2) = 1.040$, $d(NH) = 1.024$; $D(NO_1) = 2.670$, $D(NO_2) = 2.892$; $D(O_1O_3) = 2.754$, $D(O_2O_3) = 2.915$; $\angle NH_1O_1 = 160.13$, $\angle NH_2O_2 = 162.24$; $\angle O_1HO_3 = 134.74$, $\angle O_3HO_2 = 134.86$; $\angle H_1NH_2 = 107.20$	
3V	$d(NH_1) = 1.037$, $d(NH_2) = 1.037$, $d(NH_3) = 1.036$, $d(NH) = 1.022$; $D(NO_1) = 2.772$, $D(NO_2) = 2.774$, $D(NO_3) = 2.775$; $D(O_1O_2) = 2.876$, $D(O_2O_3) = 2.871$, $D(O_3O_1) = 2.868$; $\angle NH_1O_1 = 134.72$, $\angle NH_2O_2 = 134.32$, $\angle NH_3O_3 = 133.20$; $\angle O_2HO_2 = 124.89$, $\angle O_2HO_3 = 125.37$, $\angle O_3HO_1 = 125.32$; $\angle H_1NH_2 = 105.73$, $\angle H_2NH_3 = 105.84$, $\angle H_3NH_1 = 105.79$	$d(NH_1) = 1.034$, $d(NH_2) = 1.034$, $d(NH_3) = 1.034$, $d(NH) = 1.023$; $D(NO_1) = 2.788$, $D(NO_2) = 2.789$, $D(NO_3) = 2.790$; $D(O_1O_2) = 2.870$, $D(O_2O_3) = 2.875$, $D(O_3O_1) = 2.871$; $\angle NH_1O_1 = 133.32$, $\angle NH_2O_2 = 133.41$, $\angle NH_3O_3 = 133.36$; $\angle O_1HO_2 = 124.59$, $\angle O_2HO_3 = 124.61$, $\angle O_3HO_1 = 124.41$; $\angle H_1NH_2 = 106.23$, $\angle H_2NH_3 = 106.24$, $\angle H_3NH_1 = 106.23$
3VI	$d(NH_1) = 1.095$, $d(NH) = 1.025$; $D(NO_1) = 2.612$; $D(O_1O_2) = 2.634$, $D(O_2O_3) = 2.760$; $\angle NH_1O_1 = 175.02$; $\angle O_1HO_2 = 170.99$, $\angle O_2HO_3 = 178.35$	$d(NH_1) = 1.072$, $d(NH) = 1.025$; $D(NO_1) = 2.656$; $D(O_1O_2) = 2.679$, $D(O_2O_3) = 2.797$; $\angle NH_1O_1 = 175.18$; $\angle O_1HO_2 = 169.65$, $\angle O_2HO_3 = 179.43$

[a] The bond lengths are in unit of angstroms and angles in degrees. The numbering of the H atoms on NH_4^+ follows that of H_2O hydrogen bonded to them.

isomer **4IX**, with the ion core situated in the middle, is more stable than its analog, **4X**, by 1.58 (1.58) kcal/mol. In **4X**, a 3°H_2O can also be found. Although this species is the second least stable isomer of all $NH_4^+(H_2O)_4$ presently considered, it maintains a relatively high bonding energy of 8.40 (8.24) kcal/mol for the 3°H_2O molecule.

Isomer **4VIII** is the highest in energy of all the species illustrated in Figure 4. This isomer, similar to **3IV** and **4IV** in that it contains an AA−1°H_2O, was not favored by the MP2/6-31+G* calculations. This occurs because the approach of the fourth H_2O to 3IV can effectively open the ring, producing isomers **4IX** and **4X**. While isomer **4VIII** has the same number of N−H···O and O−H···O hydrogen bonds as **4VII**, the difference in arrangement of the water molecules results in a large deviation in stability between them.

A.5. $NH_4^+(H_2O)_5$. Figure 5 illustrates the isomeric structures of $NH_4^+(H_2O)_5$ predicted by the present calculations. Isomers **5I**−**5VI** have a complete solvation shell whereas the solvation in **5VII**−**5IX** is incomplete with one dangling NH bond exposed. As previously noted, the O−H···O hydrogen bonds which produce the outer shell are no longer coplanar with the H_2O molecules in these isomers. The formation of these hydrogen bonds is, thus, predominantly governed by the interaction of H_2O dipoles with the oxygen electron lone pairs of the solvent molecules. Formed by attaching the fifth H_2O to **4I**, isomers **5I**, **5II**, and **5III** have been previously identified by vibrational predissociation spectroscopy of $NH_4^+(H_2O)_5$ in a supersonic jet.[6] From systematic temperature dependence measurements, isomer **5II** is found be the most abundant form of the clusters at low temperatures. The present calculations predict that the ring-closed isomer with an AA−2°H_2O is 0.70 (0.86) kcal/mol lower in energy than the ring-opened one, consistent with the observations. The finding that isomer **5I** is less stable than **5II**, which is reversed in stability compared to its analogs (**3I**, **3II**) and (**4I**, **4II**), is interesting.

The intriguing ring closing process, **5I** → **5II**, is expected to occur rapidly, since it requires only bond rotation to establish the O−H···O connection. This process, however, is not favored by entropy effects at higher cluster temperatures. To better understand the isomeric transition, we calculated the transition state of **4I** → **4II** at the B3LYP/6-31G* level. This transition, instead of **5I** → **5II**, was chosen to minimize the computational time but still obtain meaningful physical insight into the ring-closing process. It is found that the isomeric transition **4I** → **4II** has a barrier height of less than 1 kcal/mol. The transition state has a geometry similar to that of the ring-open form, but with one of the two OH bonds of the 2°H_2O pointing toward the electron lone pairs of 1°H_2O after bond reorientation. In this exothermic process, the instability arising due to hydrogen bond distortion in **4II** is compensated by the interaction energy increase due to the additional O−H···O hydrogen bond formation. The energy involved in this ring formation smoothly decreases from 11.05 (10.45) kcal/mol of (**2I** + H_2O → **3II**) to 9.22 (9.03) kcal/mol of (**4I** + H_2O → **5II**), indicating that the hydrogen bonding of H_2O with NH_4^+ not only can alter the strength of the individual N−H···O bonds but also can influence the interaction between the 1°H_2O and 2°H_2O molecules.

The other ring-shaped isomer **5III**, which contains an AA−1°H_2O, is not energetically favored and has an interaction energy about 2 kcal/mol less than that of **5I**. The stepwise hydration energy of (**4IV** + H_2O → **5III**), which originates from the formation of the fourth N−H···O hydrogen bond, is $-\Delta E_{n-1,n}$ = 10.66 kcal/mol. The value is smaller than 10.81 (10.76) kcal/mol of (**3I** + H_2O → **4I**), but is significantly larger than 10.04 (10.00) kcal/mol of (**4II** + H_2O → **5II**), meaning that the N−H···O bonding is sensitive to how the H_2O molecules are arranged in the first and the second solvation shells.

The ion core charge delocalization effect intensifies as the solvation number increases from $n = 1$ to $n = 5$. This has been evident from earlier calculations that the individual N−H···O hydrogen bond gradually weakens as water molecules successively attach to the ion core. Such a charge delocalization creates a unique situation that the bonding between NH_4^+ and 1°H_2O is comparable in strength to that between solvent water molecules at $n = 4$. Owing to this effect, isomer **5VII** having a dangling NH bond can be one of the lowest energy structures

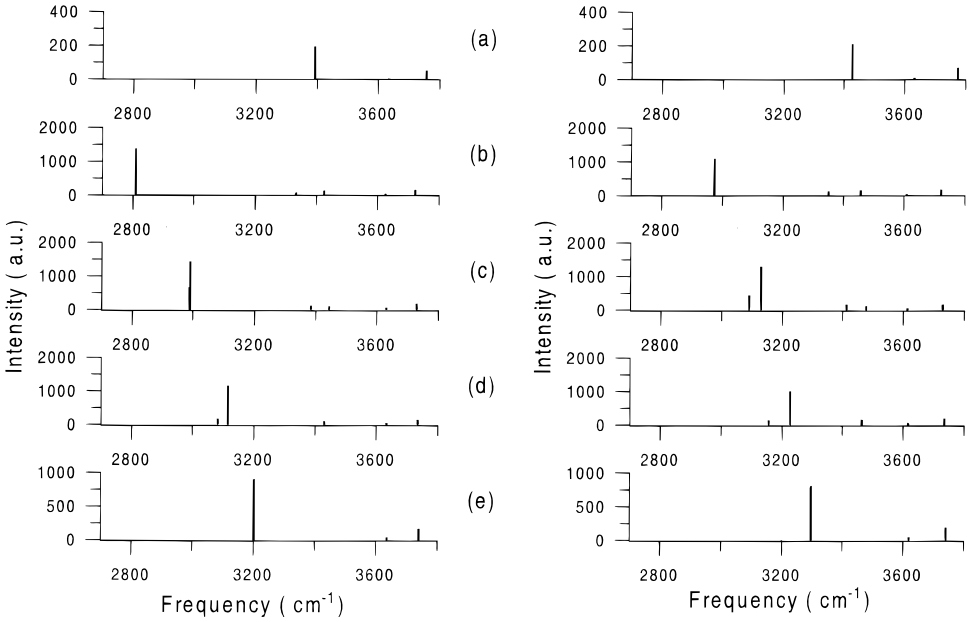

Figure 6. Vibrational stick spectra of (a) free NH_4^+ and free H_2O, and the lowest energy isomers of (b) $NH_4^+(H_2O)$, (c) $NH_4^+(H_2O)_2$, (d) $NH_4^+(H_2O)_3$, and (e) $NH_4^+(H_2O)_4$ predicted by B3LYP/6-31+G* (left) and MP2/6-31+G* (right).

of $NH_4^+(H_2O)_5$. Interestingly, this isomer contains three types of water molecules: A−H_2O (W3 and W5), AD−H_2O (W1 and W2), and AAD−H_2O (W4); it can serve as a model molecule for understanding how the frequency red shifts of free-OH stretching vibrations depend on the H_2O coordination. It is also noteworthy that isomer **5VII** is most probably produced by the hydration of **4II** or **4VII**, but not with **4I** as the precursor. This kinetics consideration has been previously employed to explain why this species was not observed in a supersonic expansion,[6b] although it is one of the lowest energy isomers. The similar competition of solvation between 1°H_2O and 2°H_2O also exists when isomer **5VIII** is formed.

The predominant isomeric forms of $NH_4^+(H_2O)_5$ depicted in Figure 5 have a structure analogous to that of $NH_4^+(H_2O)_{3,4}$. They can be produced either by covering the dangling N−H bond with H_2O or by attacking the AA−H_2O molecule of its analogs at $n = 3$ and 4. There are other ways of growing larger water clusters as well. Isomers **5IV** and **5V**, for example, are formed by hydrogen bonding H_2O to the water monomer and to the cyclic water trimer of **4V**, respectively. These two species, however, are relatively unstable. The MP2/6-31+G* calculations predict that they are comparable in energy, ∼3 kcal/mol higher than that of **5II**, but B3LYP/6-31+G* collapsed during the structural optimization of **5V**. Interestingly, the isomers (**3IV**, **4IV**, **4VIII**, **5VIII**) containing an AA−l°H_2O molecule and free NH bonds are never found by MP2/6-31+G*.

This work also considered isomer **5IX**, which owns a five-membered ring. The five-membered ring structure is somewhat similar to that found in the neutral water pentamer.[35] While this species is ∼1 kcal/mol more stable than **5III**, evidence for it was not found in the measurements.[6b]

B. Vibrational Spectra. Vibrational predissociation spectra of $NH_4^+(H_2O)_n$ revealed that more than one stable isomer could be synthesized by a free-jet expansion at $n \geq 4$.[6] Particularly at $n = 5$, a dramatic isomeric transition of **5I** → **5II** was observed at a temperature near 150 K.[6b,c] The observations strongly suggest that $NH_4^+(H_2O)_5$ can serve as a benchmark system for studying hydrogen bond rearrangement dynamics in cluster ions.[36] To assist the interpretation of the experimentally observed spectra and to perceive the spectral changes as a function of cluster sizes and structures, the predicted vibrational features in the NH and OH stretching regions are plotted in Figure 6 for $NH_4^+(H_2O)_{1-4}$ and are listed in Table 7 for $NH_4^+(H_2O)_5$. Since in these clusters, the structural isomerization is most dramatic in $NH_4^+(H_2O)_5$,[6] the following discussion concerning the spectral features and their isomeric dependence will primarily focus on the clusters with $n = 5$. A similar rationale can be applied in discussing $NH_4^+(H_2O)_{1-4}$ and larger clusters when necessary.

B.1. $NH_4^+(H_2O)_{1-4}$. Figure 6 illustrates the calculated spectra of free H_2O, NH_4^+, and $NH_4^+(H_2O)_n$ at $n = 1-4$ where all the water molecules are hydrogen-bonded to the ion core. Both the MP2/6-31+G* and B3LYP/6-31+G* calculations indicate that the frequency shift of the b-NH stretching is substantially larger than that of the f-NH. The red shifts, however, decrease smoothly with *n*, an indication of N−H···O bond weakening as *n* increases. Notably, such a decrease in red shifts correlates well with the previously discussed changes in b-NH bond lengths, N−H···O distances, and the N−H···O hydrogen bonding energies at $n = 1-4$. All these changes lead to the same conclusion that, as the number of N−H···O bonds increases, both the charge delocalization and the HB anticooperative effect intensify.

The frequency shifting of f-NH and f-OH stretches lies in the same direction of b-NHs as *n* increases, although they are much smaller in magnitude. For f-OH, the resonances are located at nearly the same frequencies, i.e. ∼3630 and ∼3730 cm^{-1} for the symmetric and asymmetric stretches of A−1°H_2O in isomers **1I**−**4I**, respectively. Shown in Figure 6 is the smooth frequency increase of the symmetric stretching from 3627 (3610) cm^{-1} of **1I** to 3636 (3619) cm^{-1} of **4I**. The frequencies of the asymmetric stretching also increase with a similar measure, from 3723 (3721) cm^{-1} to 3739 (3740) cm^{-1} for isomers **1I**−**4I**. These frequencies essentially shift toward 3635.7 (3632.7) and 3756.9 (3774.1) cm^{-1} of free H_2O at a large *n*.[32] This blue shifting derives naturally from charge delocalization of the ion core upon solvation.

B.2. $NH_4^+(H_2O)_5$. Upon formation of the second solvation shell, the $NH_4^+(H_2O)_5$ spectra in the OH stretching region dramatically change. New features emerge at 3300−3600 cm^{-1}

TABLE 7: Frequencies (cm^{-1}) and Absorption Intensities (km/mol) of NH and OH Stretches of $NH_4^+(H_2O)_5$[a]

	B3LYP/6-31+G*		MP2/6-31+G*		
species	scaled frequency	intensity	scaled frequency	intensity	assignments
5I	3064.9	844.6	3158.7	438.7	bonded-NH (1)
	3179.3	441.1	3256.5	671.2	bonded-NH (2,3,4)
	3225.4	810.0	3316.7	729.2	bonded-NH (4,2)
	3226.9	804.0	3317.6	733.0	bonded-NH (3,2)
	3412.4	668.8	3464.6	542.2	bonded-OH (1)
	3637.1	37.9	3620.1	35.9	symmetric free-OH (4)
	3637.1	38.0	3620.5	37.5	symmetric free-OH (3)
	3637.5	10.8	3620.7	20.1	symmetric free-OH (2)
	3637.9	19.5	3623.8	24.5	symmetric free-OH (5)
	3714.1	108.4	3710.7	148.1	two-coordinated free-OH (1)
	3741.2	105.1	3742.3	131.2	asymmetric free-OH (3)
	3741.3	110.7	3742.8	124.1	asymmetric free-OH (4)
	3741.7	136.1	3743.2	151.2	asymmetric free-OH (2)
	3744.5	117.4	3748.6	134.2	asymmetric free-OH (5)
5II	3141.2	113.9	3200.1	36.5	bonded-NH (1,2)
	3170.7	529.6	3271.8	470.3	bonded-NH (1,2)
	3213.9	1064.9	3306.4	1002.8	bonded-NH (3,4)
	3228.2	822.9	3318.2	745.4	bonded-NH (3,4)
	3507.6	250.6	3531.3	175.4	bonded-OH (1,2)
	3528.7	483.8	3545.9	438.8	bonded-OH (1,2)
	3618.5	14.5	3600.2	3.6	symmetric free-OH (5)
	3637.4	38.7	3620.6	42.6	symmetric free-OH (3)
	3637.7	16.5	3620.7	19.1	symmetric free-OH (4)
	3717.3	127.8	3715.5	144.7	asymmetric free-OH (5)
	3718.9	254.8	3717.6	318.1	two-coordinated free-OH (1,2)
	3722.2	41.4	3722.3	67.7	two-coordinated free-OH (1,2)
	3741.4	158.3	3742.6	178.8	asymmetric free-OH (3)
	3741.5	83.4	3742.6	99.0	asymmetric free-OH (4)
5III	2949.7	986.8	3099.9	629.7	bonded-NH (1)
	3165.1	378.5	3239.5	450.2	bonded-NH (3,4)
	3208.6	913.1	3301.6	823.2	bonded-NH (3,4)
	3288.2	390.1	3355.8	453.3	bonded-NH (2)
	3371.3	744.8	3453.4	541.1	bonded-OH (1)
	3555.6	251.2	3574.1	201.4	bonded-OH (5)
	3614.4	21.7	3597.2	6.7	symmetric free-OH (2)
	3634.9	37.5	3617.8	42.2	symmetric free-OH (4)
	3635.4	23.0	3618.3	25.2	symmetric free-OH (3)
	3712.4	122.8	3710.9	140.6	asymmetric free-OH (2)
	3715.8	113.9	3717.7	164.3	two-coordinated free-OH (1)
	3722.0	164.5	3730.2	205.3	two-coordinated free-OH (5)
	3737.6	77.1	3738.6	59.4	asymmetric free-OH (3)
	3738.2	168.6	3739.1	223.0	asymmetric free-OH (4)
5IV	2952.0	1364.9	3084.7	955.9	bonded-NH (4)
	3274.1	438.1	3318.6	521.1	bonded-NH (1,3)
	3325.0	167.5	3389.6	184.2	bonded-NH (1,2,3)
	3341.0	145.0	3391.6	174.4	bonded-NH (1,2,3)
	3379.5	731.3	3441.7	588.9	bonded-OH (4)
	3501.5	28.0	3520.7	34.1	bonded-OH (1,2,3)
	3532.0	256.1	3549.8	168.4	bonded-OH (1,2,3)
	3536.5	234.4	3550.0	167.1	bonded-OH (1,2,3)
	3637.8	25.6	3624.4	27.4	symmetric free-OH (5)
	3708.2	202.1	3703.7	232.1	three-coordinated free-OH (1,2,3)
	3708.7	209.1	3703.9	230.7	three-coordinated free-OH (1,2,3)
	3710.4	22.2	3704.3	52.1	three-coordinated free-OH (1,2,3)
	3711.9	123.1	3706.6	170.3	two-coordinated free-OH (4)
	3743.6	120.1	3748.4	137.2	asymmetric free-OH (5)
5V			3202.7	77.7	bonded-NH (4)
			3287.4	871.2	bonded-NH (1)
			3327.8	516.1	bonded-NH (3)
			3401.6	182.6	bonded-NH (2)
			3431.6	707.3	bonded-OH (1)[b]
			3500.0	58.0	bonded-OH (2)
			3539.4	175.1	bonded-OH (3)
			3618.0	36.0	symmetric free-OH (4)
			3625.9	58.2	symmetric free-OH (5)
			3639.5	218.1	bonded-OH (1)[b]
			3702.7	182.2	three-coordinated free-OH (2)
			3707.2	158.1	three-coordinated free-OH (3)
			3737.1	147.7	asymmetric free-OH (4)
			3749.9	138.5	asymmetric free-OH (5)

TABLE 7: (Continued)

	B3LYP/6-31+G*		MP2/6-31+G*		
species	scaled frequency	intensity	scaled frequency	intensity	assignments
5VI	3066.8	568.8	3158.4	305.8	bonded-NH (3)
	3160.1	746.9	3247.8	711.8	bonded-NH (4)
	3255.3	509.2	3323.8	586.9	bonded-NH (1)
	3330.0	205.2	3389.2	219.5	bonded-NH (2)
	3451.3	118.9	3482.7	103.3	bonded-OH (5)
	3471.9	416.5	3503.7	309.1	bonded-OH (1)
	3508.8	371.3	3534.9	277.8	bonded-OH (3)
	3540.4	174.6	3549.5	137.2	bonded-OH (2)
	3635.6	32.4	3618.3	35.3	symmetric free-OH (4)
	3698.3	155.5	3693.1	195.4	three-coordinated free-OH (5)
	3702.3	186.8	3696.0	198.8	three-coordinated free-OH (1)
	3705.4	92.1	3699.5	147.4	three-coordinated free-OH (2)
	3727.6	144.5	3725.0	184.5	two-coordinated free-OH (3)
	3737.3	131.6	3737.8	146.8	asymmetric free-OH (4)
5VII	3045.3	661.0	3136.9	414.3	bonded-NH (1,2)
	3052.7	697.8	3169.3	573.5	bonded-NH (1,2)
	3165.4	1051.0	3258.1	1101.5	bonded-NH (3)
	3339.4	1157.1	3395.5	976.9	bonded-OH (4)
	3403.7	493.6	3447.7	388.2	bonded-OH (1,2)
	3441.5	155.6	3476.5	188.7	free-NH
	3452.7	350.1	3489.5	282.3	bonded-OH (1,2)
	3636.8	31.5	3619.8	35.0	symmetric free-OH (3)
	3641.8	28.0	3626.3	31.4	symmetric free-OH (5)
	3684.7	104.4	3678.5	140.0	three-coordinated free-OH (1)
	3719.7	234.1	3714.6	294.9	two-coordinated free-OH (1,2)
	3722.2	22.0	3718.0	36.3	two-coordinated free-OH (1,2)
	3739.4	128.3	3739.8	146.2	asymmetric free-OH (3)
	3747.0	130.1	3749.2	145.6	asymmetric free-OH (5)
5VIII	2851.0	1155.6			bonded-NH (1)
	3110.0	308.1			bonded-NH (2)
	3148.0	1233.1			bonded-NH (3)
	3309.4	929.5			bonded-OH (2)
	3331.0	636.4			bonded-OH (1)
	3439.7	106.0			free-NH
	3504.8	334.1			bonded-OH (4)
	3634.8	41.6			symmetric free-OH (3)
	3635.3	23.0			symmetric free-OH (5)
	3685.9	103.9			three-coordinated free-OH (2)
	3712.5	115.2			two-coordinated free-OH (1)
	3713.7	145.5			two-coordinated free-OH (4)
	3737.3	122.4			asymmetric free-OH (3)
	3739.2	135.2			asymmetric free-OH (5)
5IX	2898.6	1196.3	3076.5	808.4	bonded-NH (1)
	3089.7	601.6	3193.5	532.0	bonded-NH (2)
	3164.6	959.2	3270.2	963.5	bonded-NH (3)
	3338.6	848.4	3442.1	665.9	bonded-OH (1)
	3438.8	96.3	3488.6	124.3	free-NH
	3486.3	509.3	3532.8	385.7	bonded-OH (2)
	3533.8	330.5	3570.9	284.2	bonded-OH (4)
	3615.4	17.0	3614.2	4.4	symmetric free-OH (5)
	3636.3	30.6	3635.1	34.1	symmetric free-OH (3)
	3708.1	112.9	3725.3	231.1	two-coordinated free-OH (1)
	3711.9	194.2	3729.0	69.5	two-coordinated free-OH (2)
	3713.6	127.4	3729.1	227.5	asymmetric free-OH (5)
	3718.3	94.3	3741.0	158.1	two-coordinated free-OH (4)
	3739.4	128.6	3756.5	147.2	asymmetric free-OH (3)

[a] The numbering of the b-NH groups on NH_4^+ follows that of H_2O attached to them. [b] This H_2O molecule acts as a double proton donor and a double acceptor.

for hydrogen-bonded-OH stretches. Table 7 lists the calculated frequencies of the NH and OH stretches of the $NH_4^+(H_2O)_5$ isomers. Identification of these isomers is possible based upon their characteristic stretching frequencies of f-NH, b-NH, f-OH, and b-OH.

B.2.1. Free-NH Stretching. Among all the $NH_4^+(H_2O)_5$ isomers illustrated in Figure 5, only **5VII**, **5VIII**, and **5IX** possess a f-NH bond. The vibrational frequency of this NH stretch is 3442 (3477), 3440 and 3439 (3489) cm^{-1} for isomers **5VII**, **5VIII** and **5IX**, respectively. Since isomer **5VIII** contains an AA−1°H_2O while the other two have AA−2°H_2O, the minute differences between these three frequencies indicates that the free NH stretching is quite insensitive to how water molecules are arranged in the first and the second solvation shells.

B.2.2. Bonded-NH Stretching. Figure 6e displays the spectrum of isomer **4I** containing a complete hydration shell. The spectrum shows a single asymmetric b-NH stretching absorption,

which is triply degenerate, at 3201 (3296) cm^{-1}. Adding the fifth H_2O to this isomer lifts up the degeneracy, giving rise to four distinct absorptions in the spectra. For isomers **5I**−**5IX**, the frequencies of these symmetry-broken b-NH stretches can be either shifted to the blue or to the red of 3201 (3296) cm^{-1}, depending on how hydrogen-bonding nonadditivity operates. Both B3LYP/6-31+G* and MP2/6-31+G* predict a similar propensity of frequency shifts for the b-NH stretches, although their absolute frequencies differ.

The $N-H\cdots O_1$ hydrogen bond in isomer **5I** is cooperatively coupled with $O_1-H\cdots O_5$. This cooperative coupling causes the b-NH stretching of $N-H\cdots O_1$ to resonate at a frequency about 150 cm^{-1} lower than others. For the symmetric, ring-shaped isomer **5II**, the perturbations from $2°H_2O$ result in a cooperative motion of b-NH with the b-OH of $1°H_2O$. This degree of cooperativity, however, is less than that of **5I** because the perturbing $AA-2°H_2O$ is equally shared by two $1°H_2O$ molecules. It gives rise to an additional 50 cm^{-1} red shift in these two b-NH stretches, as compared to the other two b-NH bonds without ring formation. In **5III**, the perturbation from $2°H_2O$ is slightly more complicated. In addition to the cooperative motion between $N-H\cdots O_1$ and $O_1-H\cdots O_5$, the $O_5-H\cdots O_2$ hydrogen bond is also coupled in. The stretching frequency of the b-NH linked to the $1°H_2O$ (W1) is, therefore, further red shifted to 2950 (3100) cm^{-1}, which can be compared with the corresponding frequency of 3065 (3159) cm^{-1} for **5I**. In the same isomer, the $N-H\cdots O_2$ and $O_5-H\cdots O_2$ hydrogen bonds are anticooperative, thus yielding a stretching frequency of 3288 (3356) cm^{-1} for this N−H group. The arguments based upon HB cooperativity and anticooperativity can be similarly applied to account for the frequency shifts of NH stretching of other isomers.

B.2.3. Free-OH Stretching. Our previous ab initio calculations[31] demonstrated that the f-OH vibrations of H_2O in water clusters and on ice surfaces depend sensitively on the number of coordination. The f-OH stretching frequencies of 2- and 3-coordinated H_2O can differ up to 30 cm^{-1}. In Table 7, one finds the f-OH stretching frequencies of **5IV**, **5VI**, **5VII**, and **5VIII**, which possess three types of water molecules: $A-H_2O$, $AD-H_2O$ (or two-coordinated H_2O), and $AAD-H_2O$ (or three-coordinated H_2O). Their vibrations can be described in terms of symmetric and asymmetric f-OH stretching of $A-H_2O$, 2-coordinated f-OH stretching of $AD-H_2O$, and 3-coordinated f-OH stretching of $AAD-H_2O$. More importantly, they are distinct in frequencies. The present calculations predict that the asymmetric f-OH stretching of $l°H_2O$ (W3) in **5VII** resonates at 3739 (3740) cm^{-1}, which is significantly lower than 3747 (3749) cm^{-1} of $3°H_2O$ (W5). The similar difference can be found for the symmetric stretches. Note that, aside from $A-H_2O$, the $AA-H_2O$ in isomers **5II** and **5III** can also display both symmetric and asymmetric stretches. These two vibrational modes, however, have frequencies about 20 cm^{-1} red shifted from those of $A-H_2O$ because of double hydrogen-bond formation.

The f-OH stretching frequency of 2-coordinated H_2O is lower than that of the asymmetric stretch of $A-H_2O$ by ~15 cm^{-1}. This stretch has been previously found in a variety of neutral and protonated water-containing clusters.[6a,31] Depending on how hydrogen bonding is accomplished in $NH_4^+(H_2O)_5$, the frequencies can spread over the range of 3712 (3707)−3728 (3725) cm^{-1}. As for the f-OH stretching of three-coordinated H_2O, the frequencies of **5VII** and **5VIII** are predicted to be located at 3685 (3679) and 3686 cm^{-1}, respectively. They can be compared with the similar stretches of **5IV** and **5VI** that are ~20 cm^{-1} higher in frequency because of larger hydrogen bond distortion involved in these clusters. Although **5VII** is one of the lowest in energy, the three-coordinated f-OH stretching of this isomer has not yet been previously identified in experiments.[6b] Notably, the three-coordinated f-OH stretching absorption, typically situated at ~3685 cm^{-1}, is well separated from that of the two-coordinated f-OH. Both of them, furthermore, differ in frequency than the symmetric and asymmetric free-OH stretches of $A-H_2O$ and $AA-H_2O$. The distinct vibrational pattern suggests that infrared spectroscopy of f-OH stretches can be used as a sensitive probe for the location of the water molecule, either on 1°, 2°, or 3°, as well as the number of coordination of each water molecule in the clusters.[6a,31]

B.2.4. Bonded-OH Stretching. Vibrational predissociation spectroscopic measurements[6] establish that isomers **5I** and **5II** are the two most abundant forms of $NH_4^+(H_2O)_5$ synthesized in a free-jet expansion. The ring-open isomer **5I** contains one single bonded-OH whereas the ring-closed **5II** has two; hence, one and two absorptions are expected to be observed in the b-OH stretching region, respectively. Of these two isomers, the frequencies of the latter are higher owing to the anticooperative nature of the interactions between the two $O-H\cdots O$ hydrogen bonds in **5II**. The predicted b-OH stretching frequencies of **5II** are 3508 (3531) and 3529 (3546) cm^{-1}, compared to the single frequency of 3412 (3465) cm^{-1} for isomer **5I**. Interestingly, the presence of the high-frequency doublet has indeed been confirmed by the vibrational predissociation spectroscopy of isomer **5II**, which displays the symmetric and asymmetric b-OH stretches of the two coupled $AD-1°H_2O$ molecules at 3551 and 3562 cm^{-1}, respectively.[6b] It should be noted that the similar b-OH absorptions also exist for isomer **4II**, which contains an identical four-membered ring. The calculated stretching frequencies of them are 3496 (3521) and 3519 (3537) cm^{-1}, also lower than 3553 cm^{-1} observed experimentally.[6b] It is likely that the underestimation of these frequencies in the calculations, particularly in B3LYP/6-31+G*, is a result of improper choice of the scaling factors which, determined by referring to f-OH stretches, are too small for b-OH stretches. Nevertheless, both the observations and the calculations correspondingly suggest that the absorption bands centering at ~3550 cm^{-1} are the fingerprints of a symmetric four-membered ring involving an $AA-2°H_2O$ in protonated amine−water clusters.[6c]

In addition to **5II**, isomer **5III** also contains two coupled b-OH stretches. Compared to that of **5I**, the b-OH stretching of $O_1-H\cdots O_5$ ($O_5-H\cdots O_2$) is lower (higher) in frequency owing to hydrogen bonding nonadditivity. The absorptions of these two stretches are situated at 3371 (3453) and 3556 (3574) cm^{-1}, respectively. Notably, this isomer is one of the two possible candidates responsible for the experimentally observed absorption at 3376 cm^{-1}.[6b] The other candidate is isomer **5VII** which has a 3-coordinated f-OH and three b-OH stretches. Due to the additional hydrogen bond formation between $AA-2°H_2O$ and $A-3°H_2O$, the frequencies of both $O_1-H\cdots O_4$ and $O_2-H\cdots O_4$ are ~100 cm^{-1} red shifted from those of **5II**. This bonding also gives rise to the third bonded-OH absorption at 3339 (3396) cm^{-1} for the $2°H_2O$ molecule, which now plays a role as an AAD.

Finally, three bonded-OH stretching absorptions can be found in **5IX**. The isomer has a water dimer and a monomer linked by an $AA-2°H_2O$. As expected, the b-OH stretching frequency of the $1°H_2O$ (W1) involving the water dimer is lower than that involving the monomeric $l°H_2O$ (W2). The b-OH stretching of the $2°H_2O$ (W4) molecule has the highest frequency, 3534

TABLE 8: Hydration Energies, ΔH_n and ΔG_n (kcal/mol), of $NH_4^+ + nH_2O \rightarrow NH_4^+(H_2O)_n$ at 298.15 K

	B3LYP/6-31+G*		MP2/6-31+G*		exptl	
species	$-\Delta H_n$	$-\Delta G_n$	$-\Delta H_n$	$-\Delta G_n$	$-\Delta H°_n$	$-\Delta G°_n$
1I	19.77	12.70	18.50	14.68	17.3,[a] 19.9[b]	11.4,[a] 13.0[b]
2I	35.67	21.07	33.85	21.04	32.0,[a] 32.3[b]	19.6,[a] 20.5[b]
2II	32.96	17.60	30.36	16.55		
3I	48.72	27.06	46.81	26.20	45.4,[a] 44.5[b]	25.5,[a] 26.4[b]
3II	48.09	21.32	45.70	20.83		
3III	47.14	24.63	44.42	23.36		
3IV	44.56	18.38				
3V	44.17	17.54	43.73	17.99		
3VI	42.97	19.60	39.32	17.96		
4I	59.44	31.44	57.68	30.44	57.6,[a] 55.3[b]	29.6,[a] 30.3[b]
4II	60.05	27.23	57.68	26.31		
4III	58.78	29.12	55.91	28.23		
4IV	56.94	23.41				
4V	57.08	22.63	56.36	24.25		
4VI	57.56	20.63	55.94	20.60		
4VII	59.18	25.64	55.77	19.33		
4VIII	56.29	21.80				
4IX	57.87	27.70	54.40	25.88		
4X	56.33	26.12	52.75	24.14		
5I	68.62	32.07	66.24	31.34	67.3,[a] 65.9[b]	32.6,[a] 32.9[b]
5II	70.06	30.43	67.82	30.05		
5III	67.52	27.38	65.11	27.27		
5IV	67.20	24.76	65.67	25.14		
5V			65.43	25.42		
5VI	69.21	25.10	67.42	25.51		
5VII	70.55	30.75	67.23	28.48		
5VIII	68.12	26.21				
5IX	68.97	27.52	65.82	26.53		

[a] Reference 2a. [b] Reference 3.

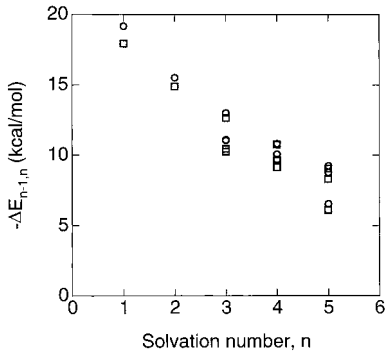

Figure 7. Calculated stepwise hydration energies ($\Delta E_{n-1,n}$) of the lowest energy isomers of $NH_4^+(H_2O)_{1-5}$ using B3LYP/6-31+G* (○) and MP2/6-31+G* (□).

(3571) cm^{-1}, of the three since it experiences HB anticooperativity and is situated furthest away from the ion core.

C. Thermodynamics. Table 8 compares the experimentally measured and the ab initio calculated $-\Delta H_n$ and $-\Delta G_n$ of the reaction $NH_4^+ + nH_2O \rightarrow NH_4^+(H_2O)_n$. Detailed comparison between them reveals that B3LYP/6-31+G* often yields larger values, whereas MP2/6-31+G* yields values in better agreement with the measurements. At $n = 1$, the variation in experimental measurements is large, up to 2.6 kcal/mol. The predicted MP2/6-31+G* value falls within this uncertainty range, but B3LYP/6-31+G* significantly overestimates the interaction energy. As for clusters of $n = 2-5$, the MP2/6-31+G* calculations for the lowest energy isomers agree well with the measurements, which have an experimental uncertainty of less than 1 kcal/mol; however, the B3LYP/6-31+G* values remain slightly overestimated. Figure 7 illustrates the evolution of the hydration energies predicted by B3LYP/6-31+G* and MP2/6-31+G* as a function of *n*. Noticeably, the difference in prediction between these two methods for the lowest energy isomers gradually diminishes as *n* increases. The estimated $\Delta E_{n-1,n}$ agrees with each other within 0.5 kcal/mol at $n = 5$, indicating that the B3LYP/6-31+G* approach is appropriate for predicting the stepwise hydration energies of clusters at a larger *n*.

Table 8 also displays the dramatic dependence of the Gibbs hydration energies on the isomeric forms of each cluster at room temperature. For the model system $NH_4^+(H_2O)_5$, the calculated energy is scattered over a wide range from $\Delta G_n = -24.76$ (-25.14) to -32.07 (-31.34) kcal/mol. The degree of scattering is substantially larger in $-\Delta G_n$ than in $-\Delta H_n$ for all the clusters considered in Table 8. This finding is not unexpected since the entropy term involved in $-\Delta G_n$ is sensitive to the temperatures as well as to the structures of the isomers. At room temperature, both the B3LYP/6-31+G* and MP2/6-31+G* calculations predict that isomer **5I**, with a ring-opened form, is lowest in Gibbs free energy. The ring-closed form is energetically favored only when the cluster is cooled off to a temperature below 160 K. Remarkably, this prediction agrees excellently well with the recent report of Wang et al.,[6b,c] who observed a distinct isomeric transition of **5I** → **5II** for $NH_4^+(H_2O)_5$ with an internal temperature of ~150 K. Since the structures of the clusters shown in Table 8 remain unknown in the hydration energy measurements,[2,3] the experimentally determined ΔH_n and ΔG_n should be considered as isomerically averaged values.

Conclusions

Both the B3LYP/6-31+G* and MP2/6-31+G* methods have been applied to investigate the geometries, energies and vibrations of $NH_4^+(H_2O)_n$ and its structural isomers at $n = 1-5$. Results indicate that charge−dipole interactions dominate the hydration of NH_4^+ in the first solvation shell whereas the arrangement of water molecules in the second hydration shell is predominantly determined by the interactions between $1°H_2O$ dipoles and the O electron lone pairs of $2°H_2O$. There is no abrupt change in $\Delta H_{n-1,n}$ at $n = 4$ and 5 as the stepwise hydration energies ($\Delta H_{n-1,n}$) decrease monotonically with *n*. The prediction is in line with previous thermochemical measurements[2,3] and the recent spectroscopic identification of structural isomers at $n \geq 4$ by Wang et al.[6] The emergence of structural isomers at $n = 4$ can be attributed to the fact that the strength of the interaction between the ion core and the solvent molecules is comparable to that between solvent molecules as the second hydration shell starts to form.

Dependence of the OH stretching frequency shifts on the solvation number in $NH_4^+(H_2O)_n$ has been scrupulously investigated in this study. The results indicate that the free-OH stretches, in addition to bonded-OH stretches, contain such useful structural information that A−H_2O, AD−H_2O, AA−H_2O, and AAD−H_2O can be identified on the basis of their characteristic free-OH stretching frequencies. While much structural information is expected to be extracted from b-NH stretches, unfortunately, the experimentally observed spectra are congested in this region,[6b] disallowing unambiguous spectral assignments.

The present calculations reveal that the geometries, interaction energies and vibrational frequencies of the clusters are strongly influenced by the hydrogen bond cooperative effect. The cooperative interactions, with the bridging molecule acting both as a proton donor and as an acceptor, can greatly enhance the strength of the involved hydrogen bonds. This enhancement, lengthening the b-NH (b-OH) bonds but shortening the N−H···O (O−H···O) distances, results in a larger frequency red shift in the b-NH (b-OH) stretches, as compared to the noncooperative case. On the contrary, in anticooperative systems where

the bridging molecule acts as a double proton donor or as a double acceptor, the b-NH (b-OH) bond lengths are substantially decreased, and the N−H···O (O−H···O) distances are, accordingly, increased.

We conclude from systematic comparisons of the present calculations that MP2/6-31+G* is a better method than B3LYP/6-31+G* in predicting the interaction energy of NH_4^+ and H_2O. It yields results in close agreement with the measurements whereas the B3LYP/6-31+G* calculations tend to overestimate the interaction energies. The MP2 method, however, is disadvantageous in that it requires more disk space when calculating the vibrational frequencies of larger clusters. The B3LYP/6-31+G* can be an alternative in this case since the DFT-predicted interaction energies agree well with those of MP2/6-31+G* at a larger *n*. The DFT approach, as pointed out by other authors, can indeed provide a reliable and computationally less demanding method for investigating intramolecular[37] and intermolecular hydrogen bonding in molecules and clusters.[38] The present study has demonstrated that this approach can also be applied to enhance our understanding of ion−molecule interactions in cluster ions generated in the gas phase.

Acknowledgment. The authors thank the Academia Sinica and the National Science Council (Contract NSC 87-2113-M-001-027-CT and NSC 87-2113-M-001-036) of Taiwan, Republic of China, for financial support. We also thank Dr. A. M. Mebel for useful discussions.

References and Notes

(1) See the special issue of *Faraday Discuss.* **1996**, *103.*

(2) (a) Payzant, J. D.; Cunningham, A. J.; Kebarle, P. *Can. J. Chem.* **1973**, *51*, 3242; (b) Kebarle, P. *Annu. Rev. Phys. Chem.* **1977**, *28*, 455 and references therein.

(3) Meot-Ner, M. *J. Am. Chem. Soc.* **1984**, *106*, 1265 and references therein.

(4) Lisy, J. M. *Int. Rev. Phys. Chem.* **1997**, *16*, 267 and references therein.

(5) For example, see: (a) Yeh, L. I.; Okumura, M.; Myers, J. D.; Price, J. M.; Lee, Y. T. *J. Chem. Phys.* **1989**, *91*, 7319. (b) Ayotte, P.; Bailey, C. G.; Weddle, G. H.; Johnson, M. A. *J. Phys. Chem. A* **1998**, *102*, 3067; (c) Choi, J. H.; Kuwata, K. T.; Cao, Y. B.; Okumura, M. *J. Phys. Chem. A* **1998**, *102*, 503.

(6) (a) Wang, Y.-S.; Jiang, J. C.; Cheng, C.-L.; Lin, S. H.; Lee, Y. T.; Chang, H.-C. *J. Chem. Phys.* **1997**, *107*, 9695; (b) Wang, Y.-S.; Chang, H.-C.; Jiang, J. C.; Lin, S. H.; Lee, Y. T.; Chang, H.-C. *J. Am. Chem. Soc.* **1998**, *102*, 8777. (c) Chang, H.-C.; Wang, Y.-S.; Lee, Y. T.; Chang, H.-C. *Int. J. Mass Spectrom. Ion Processes* **1998**, *180*, 91.

(7) Armstrong, D. A.; Rauk, A.; Yu. D. *Can. J. Chem.* **1993**, *71*, 1368.

(8) Kassab, E.; Evleth, E. M.; Hamou-Tahra, Z. D. *J. Am. Chem. Soc.* **1990**, *112*, 103.

(9) (a) Welti, M.; Ha, T.-K.; Pretsch, E. *J. Chem. Phys.* **1985**, *83*, 2959. (b) Jaroszewski, L.; Lesyng, B.; McCammon, J. A. *J. Mol. Struct. (THEOCHEM)* **1993**, *283*, 57. (c) Jaroszewski, L.; Lesyng, B.; Tanner, J. J.; McCammon, J. A. *Chem. Phys. Lett.* **1990**, *175*, 282. (d) Pullman, A.; Claverie, P.; Cluzan, M.-C. *Chem. Phys. Lett.* **1985**, *117*, 419. (e) Pullman, A.; Armbruster, A. M. *Int. J. Quantum Chem.* **1977**, *11*, 701.

(10) Contador, J. C.; Aguilar, M. A. Olivares del Valle, F. *J. Chem. Phys.* **1997**, *214*, 113.

(11) Bueker, H.-H.; Uggered, E. *J. Phys. Chem.* **1995**, *99*, 5945.

(12) Newton, M. D.; Ehrenson, S. *J. Am. Chem. Soc.* **1971**, *93*, 4971.

(13) Glendening, E. D.; Feller, D. *J. Phys. Chem.* **1995**, *99*, 3060.

(14) Magnusson, E. *J. Phys. Chem.* **1994**, *98*, 12558.

(15) Kim, J.; Lee, S.; Cho, S. J.; Mhin, B. J.; Kim, K S. *J. Chem. Phys.* **1995**, *102*, 839.

(16) Bauschlicher, C. W.; Langhoff, S. R.; Partridge, H.; Rice, J. E.; Komornicki, A. *J. Chem. Phys.* **1991**, *95*, 5142.

(17) Feller, D.; Glendening, E. D.; Kendall, R. A.; Peterson, K. A. *J. Chem. Phys.* **1994**, *100*, 4981.

(18) Xie, Y.; Remington, R. B.; Schaefer, H. F. *J. Chem. Phys.* **1994**, *101*, 4878.

(19) Bagno, A.; Conte, V.; Furia, F. D.; Moro, S. *J. Phys. Chem. A* **1997**, *101*, 4637.

(20) Bieske, E. J.; Maier, J. P. *Chem. Rev.* **1993,** *93*, 2603.

(21) (a) Jiang, J. C.; Tsai, M.-H. *J. Phys. Chem. A* **1997**, *101*, 1982. (b) Dibble, T. S.; Francisco, J. S. *J. Chem. Phys.* **1996**, *100*, 459. (c) Tsuzuki, S.; Uchimaru, T.; Tanabe, K. *Chem. Phys. Lett.* **1995**, *246*, 9. (d) Sosa, C.; Lee, C. *J. Chem. Phys.* **1993**, *98*, 8004. (e) Stephens, P. J.; Devlin, F. J.; Chabalowski, C. F.; Frisch, M. J. *J. Phys. Chem.* **1994**, *98*, 11623. (f) Gonzalez, A. I.; Mo, O.; Yanez, M.; Leon, E.; Tortajada, J.; Morizur, J. P.; Leito, I.; Maria P.-C.; Gal, J. F. *J. Phys. Chem.* **1996**, *100*, 10490. (g) Hillebrand, C.; Klessinger, M.; Eckert-Maksic, M.; Maksic, Z. B. *J. Phys. Chem.* **1996**, *100*, 9698. (h) Boesch, S. E.; Grafton, A. K.; Wheeler, R. A. *J. Phys. Chem.* **1996**, *100*, 10083. (i) Oie, T.; Topol, I. A.; Burt, S. K. *J. Phys. Chem.* **1995**, *99*, 905. (j) Kim, K.; Jordan, K. D. *J. Phys. Chem.* **1994**, *98*, 10089. (k) Lee, C.; Chen, H.; Fitzgerald, G. *J. Chem. Phys.* **1994**, *101*, 4472. (l) Laasonen, K.; Klein, M. L. *J. Phys. Chem.* **1994**, 98, 10079. (m) Sim, F.; St-Amant, A.; Papai, I.; Salahub, D. R. *J. Am. Chem. Soc.* **1992**, *114*, 4391. (n) Novoa, J. J.; Sosa, C. *J. Phys. Chem.* **1995**, *99*, 15837.

(22) Wayne, R. P. *Chemistry of Atmospheres;* Oxford University Press: Oxford, 1991.

(23) (a) Guo, H.; Karplus, M. J. *Phys. Chem.* **1992**, *96*, 7273. (b) Guo, H.; Karplus, M. *J. Phys. Chem.* **1994**, *98*, 7104.

(24) (a) Suhai, S. *J. Chem. Phys.* **1994**, *101*, 9766. (b) Suhai, S. *J. Phys. Chem.* **1996**, *100*, 3950.

(25) Edison, A. S.; Weinhold, F.; Markley, J. L. *J. Am. Soc. Chem.* **1995**, *117*, 9619.

(26) Karpfen, A. *J. Phys. Chem.* **1996**, *100*, 13474.

(27) King, B. F.; Weinhold, F. *J. Chem. Phys.* **1995**, *103*, 333.

(28) Cruzan, J. D.; Braly, L. B.; Liu, K.; Brown, M. G.; Loeser, J. G.; Saykally, R. J. *Science* **1996**, *271*, *59.*

(29) Frisch, M. J.; Trucks, G. W.; Schlegel, H. B.; Gill, P. M. W.; Johnson, B. G.; Robb, M. A.; Cheeseman, J. R.; Keith, T.; Petersson, G. A.; Montgomery, J. A.; Raghavachari, K.; Al-Laham, M. A.; Zakrzewski, V. G.; Ortiz, J. V.; Foresman, J. B.; Cioslowski, J.; Stefanov, B. B.; Nanayakkara, A.; Challacombe, M.; Peng, C. Y.; Ayala, P. Y.; Chen, W.; Wong, M. W.; Andres, J. L.; Replogle, E. S.; Gomperts, R.; Martin, R. L.; Fox, D. J.; Binkley, J. S.; Defrees, D. J.; Baker, J.; Stewart, J. P.; Head-Gordon, M.; Gonzalez, C.; Pople, J. A. *Gaussian 94*, Revision D.3, Gaussian, Inc.: Pittsburgh, PA, 1995.

(30) Boys, S. F.; Bernardi, F. *Mol. Phys.* **1970**, *19*, 553.

(31) Jiang, J. C.; Chang, J. C.; Wang, B. C.; Lin, S. H.; Lee, Y. T.; Chang, H.-C. *Chem. Phys. Lett.* **1998**, *289*, 373.

(32) Jiang, J. C. Unpublished calculations.

(33) Masella, M.; Flament, J. P. *J. Chem. Phys.* **1998**, *108*, 7141.

(34) In the study of linear pyrrole trimers (Jiang, J. C. Ph.D. Dissertation, National Taiwan University, Taipei, 1994), we found that the interaction via π-type hydrogen bonding is cooperative when the middle pyrrole molecule acts both as a proton donor and as an acceptor. The interaction is anticooperative when the middle pyrrole behaves like a double-proton acceptor.

(35) Liu, K.; Brown, M. G.; Cruzan, J. D.; Saykally, R. J. *Science* **1996**, *271*, 62.

(36) Wales, D. J.; Ohmine, I. *J. Chem. Phys.* **1993**, *98*, 7257.

(37) Lozynski, M.; Rusinska-Roszak, D.; Mack, H.-G. *J. Phys. Chem. A* **1998**, *102*, 2899.

(38) Xantheas, S. S. *J. Chem. Phys.* **1995**, *102*, 4505.